

# Fluctuation level bursts in a model of internal transport barrier formation

D. López-Bruna, D. E. Newman, and B. A. Carreras  
Oak Ridge National Laboratory, Oak Ridge, Tennessee 37831-8071

P. H. Diamond  
University of California at San Diego, La Jolla, California 92093-0319

(Received 14 July 1998; accepted 23 November 1998)

A model of internal transport barriers (ITB) is developed that, in addition to the typical features of ITB models (the phase transition character with a power threshold, barrier front propagation, etc.), exhibits an oscillatory/bursty behavior close to the transition. This behavior comes from the competition between the driving and suppression mechanisms for the turbulence. The onset of the oscillations has a power threshold,  $P_{osc}$ , below the power threshold for the transition to the enhanced confinement regime,  $P_{th}$ . In the calculations,  $P_{osc} \sim 0.5P_{th}$ . This suggests that the oscillations avoid an early transition at  $P_{th} = P_{osc}$ , so any mechanism that eliminates the oscillations may lower the transition power. © 1999 American Institute of Physics. [S1070-664X(99)00903-9]

## I. INTRODUCTION

The experiments on tokamak plasmas driven to a high confinement regime originated in 1982 in the Axisymmetric Divertor Experiment (ASDEX) tokamak.<sup>1</sup> This discovery led to a series of experiments aimed at reaching and controlling new regimes of enhanced confinement that are characterized by a decrease of the plasma edge fluctuations and the consequent formation of an edge transport barrier. Several theories were developed to model the dynamics of the process based on key experimental observations like its phase transition nature,<sup>2</sup> the correlation between the fluctuation suppression and the formation of a radial electric field ( $E_r$ ) shear layer,<sup>3</sup> and the independence of these features on the type of machine and heating mechanism.<sup>4</sup> Currently, the most accepted cause for the transport improvement is the reduction or stabilization of turbulence by sheared  $E \times B$  flow. Some model realizations of this hypothesis<sup>5,6</sup> have led to bifurcation scenarios, where a power threshold for the transition to high confinement can be estimated. The general assumptions of these are such that they can be extended to explain the basic features of the internal transport barriers (ITB).<sup>7-9</sup> Thus, several models base the formation of ITB on the same mechanism of turbulence reduction via a sheared radial electric field.<sup>10,11</sup> As happens with the edge transport barriers, the system reacts to the extra free energy supply by adjusting itself to reduce the transport. It is important to understand the key dynamical processes that lead to this reorganization in order to gain access to these regimes to control the confined plasmas. In this respect, the advantage of studying ITB formation is that the physics are independent of edge effects like wall conditioning or divertor/limiter physics. Recent reviews on transport barrier formation and related issues can be found in Refs. 12, 13, and 14.

It has been observed experimentally that there are bursts in the fluctuation level accompanying the processes of internal<sup>15</sup> and edge<sup>16</sup> transport barrier formation. In the case of the reverse shear (RS) discharge presented in Ref. 15, the bursts in the density fluctuation level coincide with a prox-

imity between the shearing rate and the estimated linear growth rate. Furthermore, the analogous discharge with reduced bursts bifurcates into an enhanced RS regime. Such fluctuation bursts have also been observed in three-dimensional turbulence models of transition based on self-generated sheared flow.<sup>17</sup> The results from these experiments support the idea of a competition between the driving and the suppression mechanisms for the turbulence. In this paper, we identify an oscillatory mechanism that is caused by the competition between the driving and suppression terms in the time evolution of the turbulence. We use an equation for the envelope of the density fluctuation level, so the oscillations referred to in this work should be understood as bursts of the rms fluctuation level itself. As will be discussed later, the model oscillations show a fairly broad power spectrum.

The transition model is based on the general assumption that the shear in the  $E \times B$  flow is able to suppress the turbulence. The  $E \times B$  shear is produced by the steepening of thermodynamic profiles of the system (e.g., the plasma pressure) and by the sheared rotation. The thermodynamic gradients are also the source of free energy driving several instabilities. Thus, the steepening of the profiles under the effect of the external sources of heat and particles is both the drive for the turbulence and its quenching. If there is a different dependence of the drive and suppression mechanisms on the pressure profile, the particle and heat fluxes can exhibit a nonmonotonic function of the thermodynamic gradients (i.e., there is an unstable range of decreasing flux for increasing gradients). When the power input makes the system reach the unstable gradients, the diffusivities are reduced in such a way that much higher gradients stand in equilibrium for the same flux. As a consequence, threshold fluxes mark the transition from/to a high confinement to/from a low confinement regime.<sup>18</sup>

The  $E \times B$  flow depends on the pressure gradient and, consequently, its shear incorporates the curvature of the pressure profile. This is important both in the process of barrier formation and in the oscillatory behavior. The poloidal<sup>19</sup> and

toroidal<sup>20,21</sup> flows may also play an important role in the suppression of the turbulence. In particular, the poloidal flow evolution can also give rise to oscillatory phenomena (Ref. 17). Here we shall focus on the role of the diamagnetic contribution to the radial electric field.

Because the modification of the transition threshold is found to be the result of the bursts in the turbulence, an understanding of their cause may help to find routes to the high confinement regimes with lower power thresholds. This work is devoted to describing numerically how the bursts can appear in a phase transition model for transport barrier formation. The paper has been organized as follows: in Sec. II we give a quick survey of the transition model, summarizing the main general results; in Sec. III we describe the oscillatory behavior observed in numerical calculations; in Sec. IV we give an insight into the generation and dynamics of the oscillatory behavior; and Sec. V is the conclusions and summary.

## II. TRANSITION MODEL

The description of the transition model is given in three parts: (a) the evolution of the density fluctuation level  $\epsilon$ ; (b) the  $\epsilon$ -dependent transport coefficients; and (c) the transport equations, which are linked to  $\epsilon$  through the transport coefficients.

### A. Evolution of the density fluctuation level $\epsilon$

The transition mechanism is based on the notion of competition between the rates of growth of the turbulence caused by gradient-driven instabilities and of its decorrelation via electric field shear.<sup>22</sup> Here, we adopt the “turbulence” field  $\epsilon \equiv \langle (\tilde{n}/n_0)^2 \rangle^{1/2}$ , which represents the envelope of the density fluctuations.<sup>21</sup> The time evolution of  $\epsilon$  depends on three main components. First, in the absence of any suppression mechanism, the fluctuation level is assumed to have a linear drive that depends on the particular instability considered. Second, this growth is limited by the typical turbulent saturation mechanism, the convective nonlinearities in the turbulent (low confinement) state, which we represent by an  $\epsilon^2$ -dependent term. The third component is the fluctuation suppression term, associated with the radial electric field shear. Including a diffusive term, the general form for the time evolution of  $\epsilon$  is then

$$\begin{aligned} (\text{evolution}) &= (\text{linear drive}) - (\text{saturation}) \\ &\quad - (\text{suppression}) + (\text{diffusion}). \end{aligned}$$

Following this scheme we have, in cylindrical coordinates,

$$\frac{\partial \epsilon}{\partial t} = \left( \gamma - \alpha_1 \epsilon - \frac{\omega_s^2}{\gamma} \right) \epsilon + \frac{1}{r} \frac{\partial}{\partial r} \left( r D_\epsilon \frac{\partial \epsilon}{\partial r} \right), \quad (1)$$

where  $\gamma$  is the linear growth rate for the particular instability and  $D_\epsilon$  is the turbulence diffusivity.<sup>23</sup> The coefficient  $\alpha_1$  of the saturation term is taken generically as  $\alpha_1 = (\bar{k}_\theta \rho_s) c_s / \Delta$ , where  $k_\theta$  is the poloidal wave number with an overbar indicating the spectral average;  $\rho_s = c_s / \Omega_i$  is the sound Larmor

radius;  $c_s = (T_e / m_i)^{1/2}$  is the ion sound velocity; and  $\Delta$  is the characteristic scale length of the turbulence, which has a functional dependence on the thermodynamic profiles according to the instability model used. From Eq. (1), the L-mode level of fluctuations in equilibrium is  $\epsilon = \gamma / \alpha_1$ , assuming that the diffusion term is not determining the  $\epsilon$  profile. In fact, it is a requirement of this transition model that the driving part in Eq. (1) is dominant, as the time scales of the fluctuation level evolution should be of the order of  $\gamma^{-1}$ . Therefore, different levels of saturation can be obtained depending on the turbulence model chosen (i.e., the  $\gamma$  and  $\Delta$ ). A list of some of the possible choices is given in Diamond *et al.*<sup>24</sup> The turbulence suppression term includes the  $E \times B$  shearing rate  $\omega_s$ . We adopt the form of the shearing rate in a tokamak,<sup>11,25</sup>  $\omega_s = (\Delta r_0 / r \Delta \theta) (r/q) (\partial/\partial r) (q V_E / r)$ , where  $q = r B_\varphi / R B_\theta$  ( $\varphi$  and  $\theta$  refer to the toroidal and poloidal components);  $V_E = |\mathbf{E} \times \mathbf{B}| / B^2$  is the  $E \times B$  flow velocity; and  $\Delta r_0$  and  $r \Delta \theta$  are the correlation lengths of the ambient turbulence in the radial and poloidal directions. Following Hahn and Burrell,<sup>25</sup> we assume that the sign of  $V_E$  does not intervene in the suppression of fluctuations. The suppression occurs when the shearing rate exceeds the decorrelation rate of the ambient turbulence. Therefore, we use the expression squared and then normalize it to the growth rate to give a threshold condition for the transition  $\omega_s \sim \gamma$  in Eq. (1). We have embedded the ratio of the correlation lengths in the coefficient  $\alpha_2$ . From scale length estimates we obtain  $\alpha_2 \sim 0.1$ . Within this order of magnitude, we use  $\alpha_2$  as a free parameter. Note that we have  $V_E \sim E_r$ , where  $E_r$  is the radial electric field, and, therefore, its radial derivative  $E_r'$  is largely responsible for changes in  $\omega_s$ .

The radial electric field  $E_r$  enters in the definition of the shearing rate. It is determined from the radial force balance equation in steady state:

$$E_r = \frac{1}{Z|e|n} \frac{\partial P}{\partial r} - V_\varphi B_\theta + V_\theta B_\varphi, \quad (2)$$

where we are assuming, in accordance with the fluid approach to the problem, that the radial force balance is achieved in a magnetohydrodynamic (MHD) time scale, faster than the diffusion time scales in the problem. In Eq. (2),  $Z$  is the charge state of the main ions,  $e$  is the electron charge,  $P$  is the ion pressure,  $V$  is the ion velocity, and  $B$  is the magnetic field.  $\varphi$  and  $\theta$  refer, respectively, to the toroidal and poloidal components. As mentioned previously, both  $V_\theta$  and  $V_\varphi$  can introduce interesting phenomena to the problem, but we shall discuss only the  $\nabla P$  contribution to  $E_r$ .

### B. $\epsilon$ -dependent transport coefficients

The anomalous transport depends on the level of fluctuations. To find this relationship, we need a model for the turbulent transport. Since we are interested in the dynamics of ITB, we need a model that relates the growth rate to the profiles of the system in the confinement region of the plasma. The  $\eta_i$  model seems to describe many of the features of L-mode plasmas.<sup>26</sup> Here we use the toroidal  $\eta_i$  model of Biglari *et al.*,<sup>27</sup> from which we obtain the main dependencies for the growth rate and the width of the instabilities:

$$\gamma \sim k_{\theta} \rho_s \frac{c_s}{a} f(\hat{s}) \left( \frac{a}{R} \right)^{1/2} \left( \frac{a}{L_n} + \frac{a}{L_T} \right)^{1/2} \left( \frac{T_i}{T_e} \right)^{1/2},$$

$$\Delta \sim \rho_s \sqrt{\frac{q}{\hat{s}}} \left[ R \left( \frac{1}{L_n} + \frac{1}{L_T} \right) \frac{T_i}{T_e} \right]^{1/4}. \quad (3)$$

Here,  $R$  and  $a$  are the major and minor radii of the tokamak;  $L_n = n(\partial n / \partial r)^{-1}$ ;  $L_T = T_i(\partial T_i / \partial r)^{-1}$ ; and  $\hat{s} = (1/q) \times (\partial q / \partial r)$  is the magnetic shear. The function  $f(\hat{s})$  parametrizes the effect of magnetic shear stabilization. The anomalous transport coefficients must be  $\epsilon$  dependent in our model. Based on the  $\eta_i$  model we write the fluctuation driven ion energy transport in the radial direction,  $\chi_i \approx \langle \tilde{v}_r \tilde{p} \rangle / (-\partial P_0 / \partial r)$ , and then relate the fluctuating pressure,  $\tilde{p}$ , and  $E \times B$  radial velocity,  $\tilde{v}_r$ , with  $\epsilon$ . The resulting anomalous part in the ion thermal conductivity is

$$\chi_{i\eta_i} = D_0 \epsilon^2 = k_{\theta} \rho_s c_s a \left( \frac{a}{R} \right)^{-1/2} \left( \frac{a}{L_n} + \frac{a}{L_T} \right)^{-1/2} \left( \frac{T_i}{T_e} \right)^{1/2} \epsilon^2, \quad (4)$$

where we have taken Eq. (3) as exact equations. In consequence, we admit a free parameter ( $\sim 1$ ) in front of Eq. (4) to adjust the transport. We obtain the electron thermal conductivity and the particle diffusivity in an analogous manner. Then we have, for each field, a transport coefficient in the form  $D = D_n + D_0 \epsilon^2$ , where  $D_n$  is a background neoclassical transport and  $D_0$  is a function of the thermodynamic profiles and their gradients obtained from the  $\eta_i$  model. The neoclassical transport, being small compared to its anomalous counterpart, has been taken to be a constant. We consider the transport coefficient  $D_{\epsilon}$  in Eq. (1) as a control of the minimum spatial scales allowed for  $\epsilon$ , which should not be less than the scale length for the turbulence, and  $D_{\epsilon}$  is taken to be constant in space and time and of the same order as the particle diffusivity.

### C. Transport equations

Equation (1) has been coupled to different sets of transport equations, ranging from a two-field ( $\epsilon$ , density) simple model to a comprehensive transport code with evolving density, ion and electron temperatures, current, toroidal and poloidal momenta, and evolving flux surfaces. However, the oscillatory features of  $\epsilon$  seem to be intrinsic to all systems when Eq. (1) is coupled to the diffusive fields through the  $\epsilon$ -dependent transport coefficients. Therefore, and for the sake of consistency, all the results presented in this paper correspond to the same system of transport equations, which has been described in detail by Newman *et al.*<sup>21</sup> It includes the electron density and the ion and electron temperature equations. There is no current evolution, and for our purposes the external sources (heat and particles) have a prescribed Gaussian shape centered at the magnetic axis. The parameters correspond to reversed shear Tokamak Fusion Test Reactor (TFTR)<sup>28</sup> discharges. To take into account the stabilizing effect of the negative shear,<sup>29</sup> we prescribed a radial function  $f(\hat{s})$  [see Eq. (3)], requiring that  $\gamma$  is lowered in the region of reverse shear by a factor  $\sim 0.1$ . As discussed by Newman *et al.*,<sup>21</sup> this causes the transition to be triggered at approximately the shear reversal position ( $q_{\min}$ ). The func-

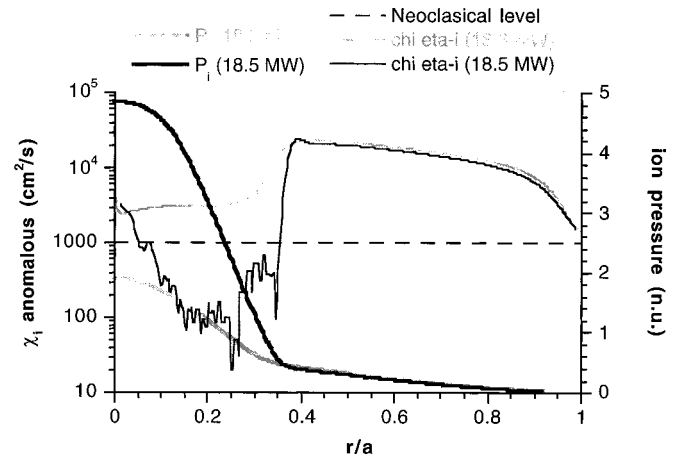


FIG. 1. Radial profiles of the pressure and the anomalous thermal conductivity  $\chi_i$  (ion channel) calculated for neutral beam injection (NBI) powers slightly below and above the threshold power for the transition. After the transition, the total  $\chi_i$  is practically reduced to its neoclassical (background) level in the region of steepest pressure gradients.

tion  $f(\hat{s})$  reflects the fact that  $\eta_i$  instabilities are greatly reduced in the reverse shear (RS) region, although not necessarily suppressed.<sup>30</sup> Therefore, the profiles steepen more rapidly in the region of RS, allowing for a larger  $\omega_s$ , where  $\gamma$  is reduced. In the context of our model this explains the benefit of RS regimes to access high confinement modes.

An example of transition with increasing power is shown in Fig. 1. The profiles correspond to the pretransition and post-transition profiles of the anomalous thermal conductivity and the pressure for a calculation in which the power was slowly ramped up. The sudden increase in the confinement is a result of the suppression of the fluctuation level (i.e., the anomalous transport) after the critical condition  $\omega_s \sim \gamma$  has been locally reached. The existence of a threshold comes from the different functional dependence of  $\omega_s$  and  $\gamma$  on the shape of  $P$ , but not on the particular dependencies. It is enough that locally  $\omega_s$  can grow faster than  $\gamma$  as the power input to the system is increased. When  $\omega_s > \gamma$ , the solution to Eq. (1) is  $\epsilon = 0$ , since  $\epsilon$  is positive definite. This automatically eliminates the anomalous transport [Eq. (4)] and the confinement improves, steepening further the pressure and causing an even larger ratio  $\omega_s^2 / \gamma^2$ . Although the  $\eta_i$  model used for these results requires an  $\epsilon^2$  dependence of the transport, a linear dependence also gives transition dynamics, as we have found with other model realizations.

Newman *et al.*<sup>21</sup> discuss in more detail some features of the transition model within this set of transport equations. These include the following: The system exhibits hysteresis, giving a lower-power threshold  $P_{\text{th}}$  for the backward transition (from high to low confinement) than for the forward transition (low to high). The time scale associated with the forward transition is found to be faster than the scale for the backward transition. Dependencies of the  $P_{\text{th}}$  have been found:  $P_{\text{th}} \sim B^\alpha$ ;  $1 < \alpha < 3$ ; and  $P_{\text{th}} \sim n$ , where  $B$  is the toroidal magnetic field and  $n$  is the line-averaged density. The different exponents  $\alpha$  depend on the relative evolution of  $T_i$  and  $T_e$ .

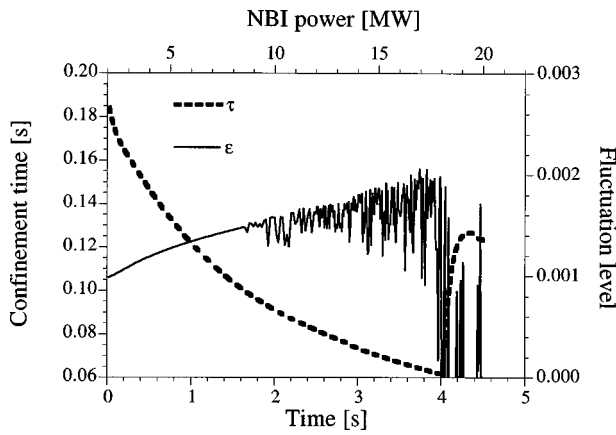


FIG. 2. Time traces of the density fluctuation level at  $r/a=0.25$  and the energy confinement time in a calculation where the neutral beam injection (NBI) power was slowly ramped up. The critical condition  $\omega_s \sim \gamma$  is met at  $P_{th} \approx 18$  MW. The oscillatory activity starts at  $P_{osc} \approx 9$  MW.

### III. OSCILLATORY BEHAVIOR

An intrinsic feature of the transition model is that the transition is preceded by oscillations in  $\epsilon$  (Fig. 2) with a power threshold  $P_{osc}$ . The possibility that these oscillations have a numerical origin was studied extensively. These studies have shown that this is not the case. One of the difficulties found is that the system tends to make use of the smallest spatial scales,  $\lambda$ , possible, which can cause grid separation problems unless a limit is set for  $\lambda$  in some way [for example, through  $D_\epsilon$  in Eq. (1)]. As noted previously,  $\epsilon$  represents the envelope of the density fluctuation level, so when we refer to oscillations in  $\epsilon$  it should be regarded as bursts in the fluctuation level. In the calculations, the oscillatory behavior starts at, roughly, half the power threshold for the transition. A systematic study of the onset condition gives  $P_{osc} = (0.50 \pm 0.09) P_{th}$ .

Figure 3 is a contour plot of the time evolution of the  $\epsilon$  profile showing these oscillations and their propagation. Initially,  $\epsilon$  is steep in the region close to the shear reversal position ( $r/a=0.35$  in this example), which coincides with

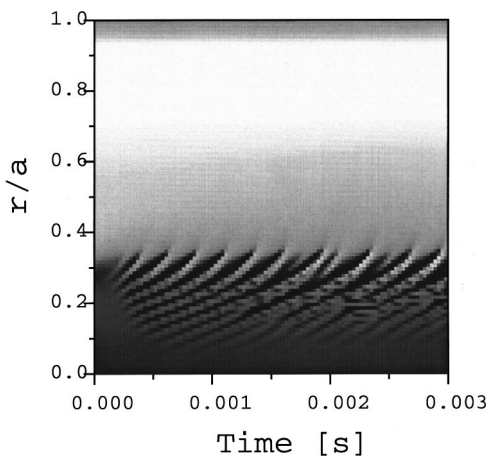


FIG. 3. Onset of the oscillations. The system is allowed to evolve from the equilibrium ( $t=0$ ) at a power slightly above  $P_{osc}$ . Data values range from zero (black) to the maximum (white).

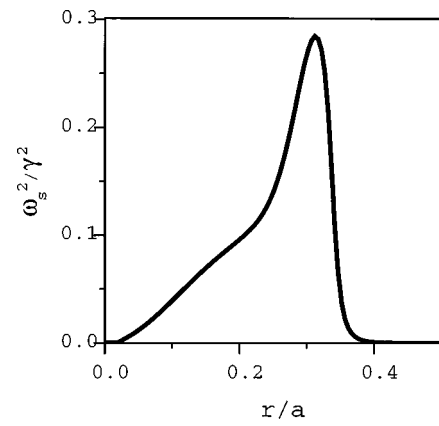


FIG. 4. The radial profile of the ratio between the driving and suppression terms in the fluctuation level evolution equation just before the onset of the oscillations.

the region of separation between low [through  $f(\hat{s})$ ] and high  $\gamma$ . The steepest gradients in the pressure profile are also found in this region, which is where the shearing rate reaches its maximum value, thus giving the maximum ratio  $\omega_s^2/\gamma^2$ . When and where the peak of the ratio (Fig. 4) reaches a threshold value, the system becomes unstable giving rise to the oscillations shown in Fig. 3. This threshold value for the maximum ratio before the oscillations start has been found to be  $\omega_s^2/\gamma^2 \approx 0.3$  in all our calculations.

The oscillations in  $\epsilon$  are translated, through the anomalous transport, into oscillations in the gradient and the curvature of the pressure profile (i.e., the ratio  $\omega_s^2/\gamma^2$  itself develops propagating oscillations). For this reason, the regions of a non-negligible ratio around the peak in the ratio (see Fig. 4) can easily reach the unstable limit after the first pulse is initiated, which implies that the point of origin of the subsequent oscillations moves inward, as illustrated in Fig. 3. The oscillations rapidly diffuse away when they reach the region of large growth rate as a result of both the enhanced transport (that tends to smooth the pressure profile) and the small shearing rate. Therefore, the radial extent of the oscillations depends on the peakedness of the ratio  $\omega_s^2/\gamma^2$ .

When the power approaches  $P_{th}$ , the ratio can surpass locally and periodically the transition threshold value  $\omega_s \sim \gamma$ . However, the fast propagation prevents the feedback mechanism from having time to build up the pressure profile enough to trigger the transition. Furthermore, the outward propagating oscillations cause an added effective transport of particles and heat across the region of steep gradients to the region of poor confinement outside  $q_{min}$  (Fig. 5). This propagation increases the power needed to reach the critical gradients. Therefore, the propagation velocity,  $V_p$ , plays an important role in delaying the formation of a transport barrier. The relation  $D_\epsilon \sim \lambda^2 f = V_p^2/f$ , where  $\lambda$  is the average wavelength of the oscillations and  $f$  is their frequency, holds reasonably well in this model [Fig. 6(a)]. On the other hand, we have  $f \sim \gamma$ , which gives a dependence close to  $V_p \sim \sqrt{D_\epsilon} \gamma$  [Fig. 6(b)].  $D_\epsilon$  sets a limit for the minimum  $\lambda$  attainable, but does not have any physical meaning otherwise. Thus,  $V_p$  is fundamentally governed by the growth rate in this model.

The data in Fig. 6(b) require some comment: At constant

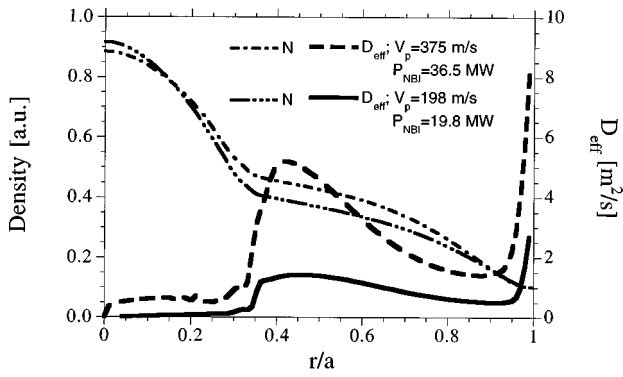


FIG. 5. Radial profiles of the density,  $n$ , and the effective particle diffusivity (calculated as  $D_{\text{eff}} = -\int r S(r) dr / \nabla n$ ) immediately before the transition for two cases characterized by different propagation velocities of the oscillations in the fluctuation level.

power we obtained  $V_p \sim D_\epsilon^{0.2 \pm 0.1}$ . However, a modification in  $D_\epsilon$  affects the transport through  $V_p$ , thus also affecting  $\lambda$ . We decided to calculate the dependencies of  $V_p$  at constant  $P_{\text{th}} - P$ , that is, constant distance to the critical point in parameter space, assuming the power as the control parameter. In this way we obtained  $V_p \sim D_\epsilon^{0.4 \pm 0.1}$  for  $P_{\text{th}} - P \approx 0$  (just before the transition) and  $V_p \sim D_\epsilon^{0.5 \pm 0.2}$  for  $P_{\text{th}} - P \approx 10$ . This last case corresponds to the data in Fig. 6.

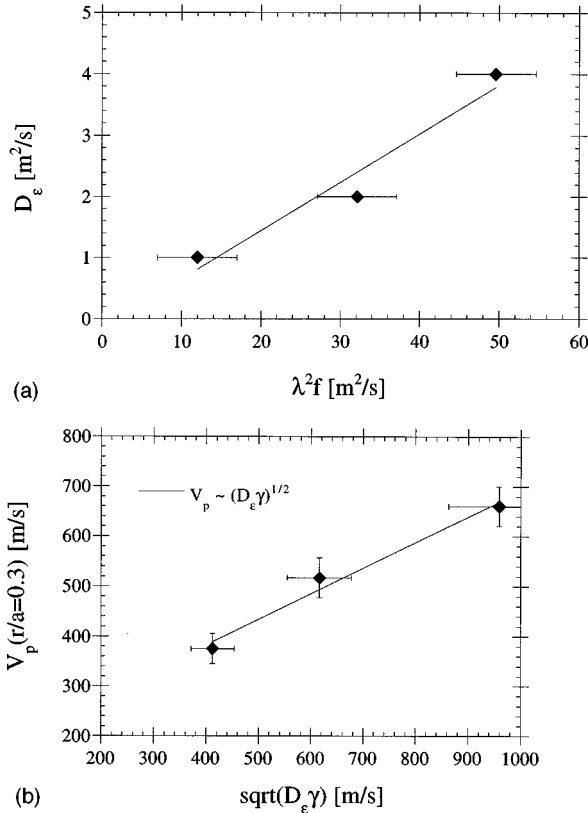


FIG. 6. (a) The relation between the diffusivity  $D_\epsilon$  and the parameter  $\lambda^2 f$ , where  $\lambda$  is the wavelength of the oscillations and  $f$  is their frequency. (b) Velocity at which the oscillations in  $\epsilon$  propagate as a function of the parameter  $\sqrt{D_\epsilon \gamma}$ , where  $\gamma$  is the local linear growth rate and  $D_\epsilon$  is the diffusivity in the  $\epsilon$ -evolution equation.

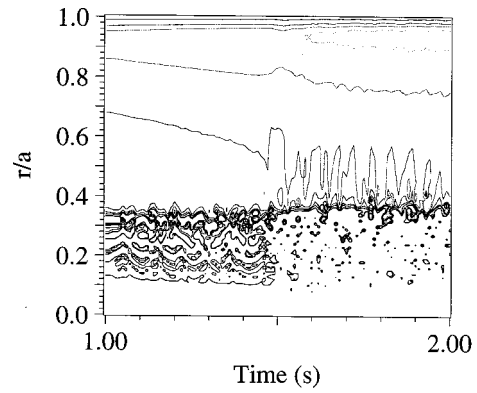


FIG. 7. A contour plot of the time evolution of the  $\epsilon$  profiles [see Eq. (1)] as the neutral beam injection (NBI) power is slowly ramped up from below to above the transition power threshold  $P_{\text{th}}$ . The transition is produced at  $t \approx 1.5$  s and is preceded by bursts in  $\epsilon$  (not resolved in this time scale) around the radial position that eventually becomes the barrier front. After the transition, the bursty behavior persists at the barrier edge.

After the transition, there is a region of suppressed  $\epsilon$  in which  $\omega_s > \gamma$ . The point where  $\omega_s \sim \gamma$  ( $r/a \sim 0.35$  in Fig. 1) limits the region of suppressed fluctuations, and can be seen as the location of the transport barrier. Therefore, just outside the transport barrier the growth rate and the shearing rate are close to each other, giving a ratio above the threshold for the onset of the oscillations. As a result, the oscillations at the barrier front should be present, even after the transition. This was numerically tested in a number of cases, one of which is shown in Fig. 7. The figure is a contour plot of the  $\epsilon$  profiles around the time of the transition ( $t = 1.5$  s) and shows both the precursor bursts around the location of near critical gradients and the bursty behavior at the barrier after the transition. Note also that, at the moment of the transition, there is a transient reduction in the fluctuation level that almost reaches the plasma edge. This is caused by a transient reduction in the fluxes when the transport barrier is formed.

From the time trace of  $\epsilon$  at the barrier front a Fourier time series analysis was performed to find the possible dependence of the frequency of the oscillations on the power. Figure 8 shows the power spectrum of  $\epsilon$  evaluated at  $r/a$

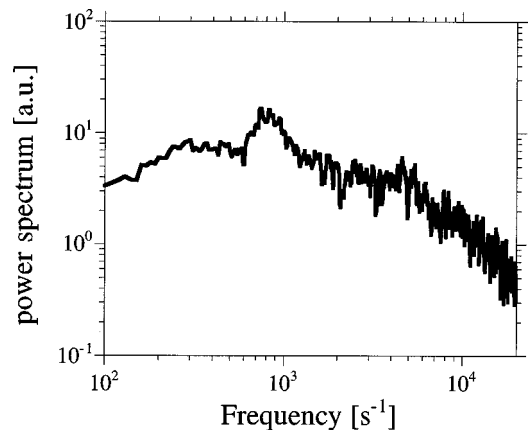


FIG. 8. The power spectrum of the time trace of  $\epsilon$  ( $r/a = 0.39$ ) at  $t = 1.6$  s (see Fig. 7). The location corresponds to the barrier front. The signal has been averaged.

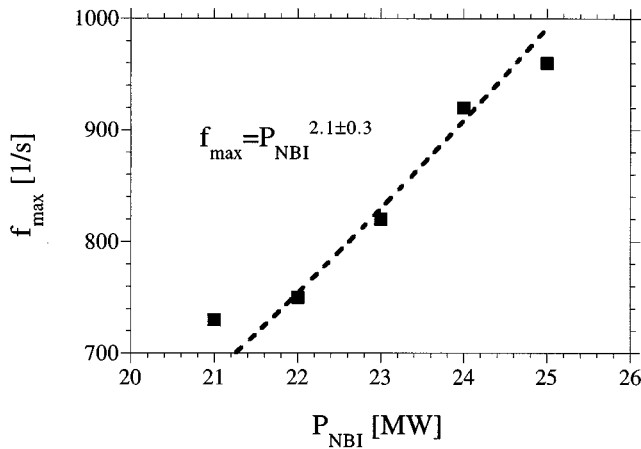


FIG. 9. Dependence of the frequency associated to the maximum amplitude in the power spectrum of  $\epsilon$ ,  $f_{\max}$ , on the neutral beam injection (NBI) power at the transport barrier front. The dashed line is a power law fit with the result shown.

$=0.39$  in Fig. 7, which is characterized by a broadband spectrum as a consequence of the strong nonlinearities of the system. Because the variable  $\epsilon$  represents the envelope of the density fluctuation level, its local frequency spectrum (Fig. 8) indicates that this envelope itself has a rather bursty behavior. When the same analysis is performed for increasing neutral beam injection (NBI) powers,  $P_{\text{NBI}}$ , the frequency associated with the maximum amplitude in the power spectrum,  $f_{\max}$ , shifts to higher values (Fig. 9). A power law fit gives  $f_{\max} \sim P_{\text{NBI}}^2$ , although the data are compatible with a linear fit. From dimensional estimates, the power flux through the transport barrier is proportional to the thermal

conductivity [Eq. (3)]. Using the saturation condition outside the barrier  $\epsilon = \gamma/\alpha_1$ , we see from Eqs. (3) and (4) that  $\gamma \sim \chi$ . As mentioned previously, there is also a roughly linear relation between  $\gamma$  and  $f$ , which explains the increase in  $f$  for increasing  $P_{\text{NBI}}$ .

#### IV. CHARACTERISTIC PROPERTIES OF THE OSCILLATIONS

The fact that there is a threshold for the onset of the oscillations independent of the transport model suggests that there is an intrinsic mechanism, provided by how Eq. (1) determines the evolution of the anomalous transport, that makes the system unstable when the shearing rate and the growth rate are close enough to each other. Two questions are addressed here: (1) What is the dynamical mechanism for the oscillations? and (2) why do the pulses propagate? To gain insight on question (1), the stability of the system has been checked by perturbing  $\epsilon$  locally and following its evolution. It is found that the imposed pulse damps away [Fig. 10(a)] with a time decay constant that decreases with the local value of the ratio  $\omega_s^2/\gamma^2$ . This decay constant eventually becomes negative [Fig. 10(b)] for values of the ratio above a threshold. These figures show the value of both  $\epsilon$  and the ratio at  $r/a=0.25$ , where the perturbation is generated. The maximum ratio in these cases corresponds to  $r/a=0.31$  and its value for the case, Fig. 10(b), was  $\omega_s^2/\gamma^2(0.31)=0.28$ . Although a negative time decay constant would cause divergent oscillations, the damping mechanisms set a limit for the amplitude. This amplitude has been found to increase with the power as well, which can be translated as a dependence between the amplitude and the value of the local time average of the ratio. Figure 11 is a plot of the

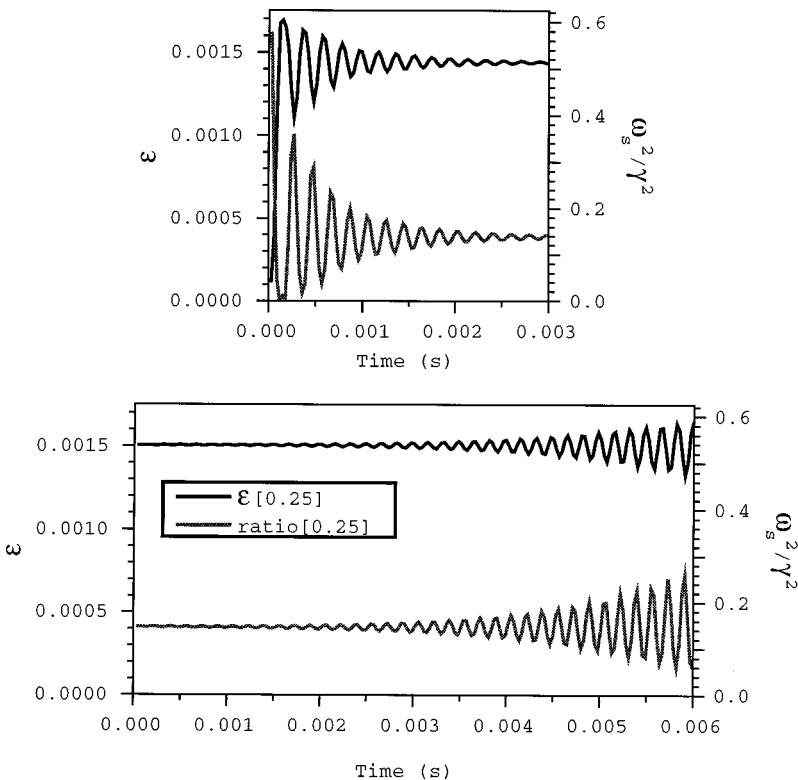


FIG. 10. The time traces of  $\epsilon$  and the ratio  $\omega_s^2/\gamma^2$  at ( $r/a=0.25$ ). Case “a” shows the relaxation of an imposed pulse in  $\epsilon$  at  $t=0$  (centered in  $r/a=0.25$ ) starting from the equilibrium slightly below the power threshold for the onset of the oscillatory behavior,  $P_{\text{osc}}$ . In case “b,” the power is increased to slightly over  $P_{\text{osc}}$  and the system becomes unstable, generating the pulses by itself (i.e., it becomes oscillating). The amplitude of these oscillations is limited by the nonlinear damping.

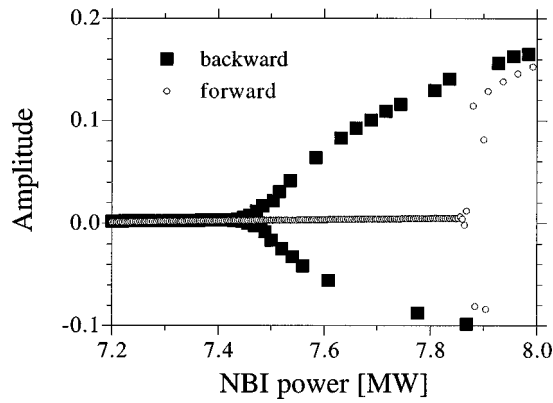


FIG. 11. The amplitude (maximum departure from the steady value) of the ratio  $\omega_s/\gamma^2$  at  $r/a=0.25$  as a function of increasing (circles) and decreasing (filled squares) neutral beam injection (NBI) power. The threshold for the onset of the oscillations is higher in the forward case, and they appear with a finite amplitude. In the backward case, the oscillations disappear from a much smaller amplitude, although it may also be finite.

amplitude of the oscillations for increasing (circles) and decreasing (filled squares) power. The plot is reminiscent of a Hopf bifurcation diagram, where there is a threshold for the onset of a finite-amplitude limit cycle and an inaccessible region that translates into the system exhibiting hysteresis. Note that the limit cycle description may apply to a feature of the system that is dominant in this small region of parameter space but that is really embedded in a more complicated dynamical system.

The explanation for the existence of the threshold  $P_{\text{osc}}$  is that the fluctuation level is able to respond to slight perturbations in the profiles only when the shearing term in Eq. (1) is close enough to the growth rate. This is a response to the feedback mechanism provided by the  $\epsilon$ -dependent anomalous transport: A perturbation in  $\epsilon$  is translated into a perturbation in the pressure profile (i.e., in its gradient), which, in turn, affects  $E_r$  [see Eq. (2)], and consequently  $\omega_s$ . The feedback is closed through Eq. (1). When the ratio is below the threshold, a perturbation in  $\epsilon$  will also affect the pressure profile, but the feedback is not strong enough to cause an amplified reaction back on the fluctuation level, in which case the perturbation decays with the relaxation of the pressure profile as shown in Fig. 10(a). It has been suggested<sup>31,32</sup> that the  $\nabla T_i$  contribution to  $\nabla P/n = \nabla T_i + (T_i/n)\nabla n$  in  $E_r$  [Eq. (2)] should be canceled by the neoclassical poloidal velocity ( $V_\theta \sim -\nabla T_i$ ) in the collisionless regime.<sup>33</sup> In this case the threshold power for the transition can increase significantly if the same suppression coefficient,  $\alpha_2$ , is used, but we have found that the oscillatory mechanism is still operative.

If the pulses could not move away from the near-critical region, the threshold for the transition would actually be  $P_{\text{osc}}$  because of the dynamo mechanism provided by the  $\nabla P$  contribution to the shearing rate, that is, once  $\epsilon$  starts to locally decrease, the local transport is reduced and the profiles build up, further increasing  $\omega_s$  with respect to  $\gamma$ . To investigate this aspect, we turn to the remaining question of what makes the pulses propagate. To clarify this we make explicit the dependencies of  $\gamma$  and  $\omega_s$  on the pressure gradient:

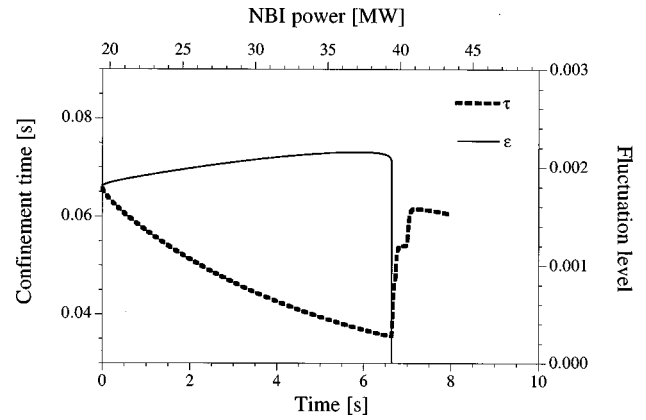


FIG. 12. Time traces of  $\epsilon$  at  $r/a=0.25$  and the energy confinement time in a calculation with the neutral beam injection (NBI) power slowly ramped up for a case without the  $\nabla^2 P$  contribution to the shearing rate.

$$\gamma \sim \sqrt{\nabla P}, \quad (5)$$

$$\omega_s \sim \left( \frac{1}{q} \frac{\partial q}{\partial r} - \frac{1}{n} \frac{\partial n}{\partial r} - \frac{1}{r} \right) \nabla P + \nabla^2 P,$$

where we have dropped the flows in Eq. (2). In a smooth function with an inflection point (like the pressure profile), there is a natural shift between the maxima for the first and second derivatives. The expressions in Eq. (5) clearly show that this can cause a shift between the maxima in  $\gamma$  and  $\omega_s$  whenever the second derivatives are not negligible compared to the first derivatives. In this case, a local increase in  $\nabla^2 P$  (an increase in  $\omega_s$ ) will cause a local reduction of the transport. This, in turn, will cause an enhancement of the local gradient (and hence of  $\gamma$ ), pushing the maxima in  $\nabla^2 P$  to both sides of the inflection point, which will shift the same mechanism to other radial locations. Obviously, this can only occur as long as the reaction in  $\omega_s$  can affect the value of  $\epsilon$  in the manner explained in the previous paragraph. In the absence of the curvature term in Eq. (5) there is no possible propagation, although the transition is still possible. An example of this is given in Fig. 12, where the term  $\nabla^2 P$  was eliminated from Eq. (5). The transition is still possible since the dependencies of  $\gamma$  and  $\omega_s$  on  $\nabla P$  in Eq. (5) are still different. Nevertheless, a much higher power is needed to reach the transition, which proves that the  $\nabla^2 P$  term is an important contribution to the shearing rate in our calculations. This is clear when Fig. 12 is compared to Fig. 2. Both calculations are similar, except that the suppression coefficient used to obtain Fig. 12 is  $\alpha_2=0.2$  instead of  $\alpha_2=0.1$  in Fig. 2. Using the same  $\alpha_2$  for cases with and without  $\nabla^2 P$  in  $\omega_s$  would give even larger differences in  $P_{\text{th}}$ . The system shows no oscillatory behavior without  $\nabla^2 P$ , but the pretransition maximum ratio  $\omega_s/\gamma$  turns out to be about the same as for the onset of the oscillations when  $\nabla^2 P$  is present. This means that, effectively, the instability limit that causes the oscillatory behavior through an amplification mechanism is now responsible for pushing the system to the transition ( $\omega_s/\gamma=1$ ) from a state with a ratio of  $\omega_s/\gamma<1$ . As suggested before, the propagation mechanism through the

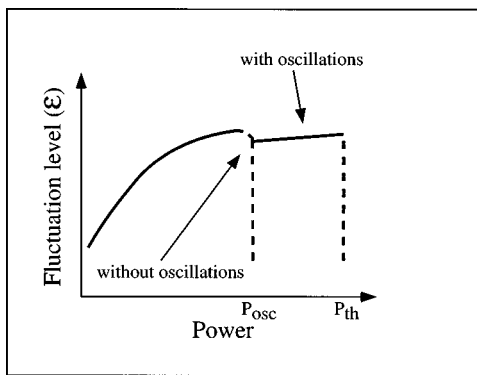


FIG. 13. Schematic variation of the local density fluctuation level as a function of the input power, depending on whether the oscillations are present.

gradient–curvature interplay protects the fluctuation level from an early rollover to the transitioned state by pushing the pulses out to the region of high  $\gamma$ , where they diffuse away very quickly. This situation is depicted in Fig. 13, where we trace schematically the local dependence of  $\epsilon$ , near the RS region, on the input power: in the absence of oscillations, the solutions with finite and null fluctuation levels are connected through only one unstable region (dashed lines) starting at  $P_{osc}$ , in which case  $P_{th} = P_{osc}$  (see also Fig. 12). If the oscillations are present, the first unstable region drives the system to the oscillatory phase, characterized by an initially lower average level of fluctuations, which can be sustained due to the effective transport caused by the oscillations themselves (see also Fig. 2). A larger power is needed to access the second phase transition.

In summary, three stable phases (low confinement, oscillatory regime, and high confinement) can be accessed using the input power as a control parameter. The schematic in Fig. 14 shows these three phases in terms of  $-\nabla P$  and the input power. As the power is increased, the local gradient increases at a rate dictated by the anomalous transport coefficients. When  $P_{osc}$  is reached, a first phase transition is characterized by an average higher pressure gradient, but still with the transport dominated by the turbulence. A further increase in the power then leads the system to the “hard” transition, characterized by a local suppression of the fluctuation level and, consequently, of the anomalous transport.

## V. CONCLUSIONS

We have reviewed, from a numerical point of view, the oscillatory behavior of the envelope of the density fluctuation level in a model of the transition to the high confinement regime based on  $E \times B$  shear flow suppression of the turbulence. In addition to the threshold for the transition, another lower threshold for the onset of oscillations in the envelope of the density fluctuation level was found in the region where the shearing rate (suppression of the turbulence) is comparable to the growth rate (drive of the turbulence). In this case, the evolution of the shearing rate can indeed affect the level of fluctuations and, therefore, the anomalous transport. This, in turn, modifies the pressure profile. There is a feedback

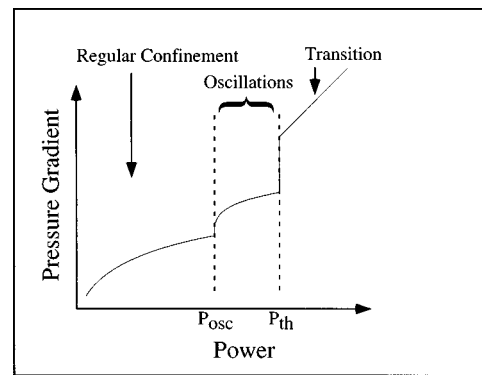


FIG. 14. Schematic representation of the variation of  $-\nabla P$  as the input power crosses the critical values  $P_{osc}$  (oscillations threshold) and  $P_{th}$  (transition threshold).

loop, caused by the nonlinear dependence of the shearing rate on the pressure profile, that can be positive for a given closeness between the rates of shearing and growth. In this case, there is an amplification process limited by the nonlinear damping in the fluctuation level evolution equation. It causes perturbations that propagate from the critical region, generating oscillations with a speed that depends mainly on the local growth rate,  $V_p \sim \gamma^{1/2}$ . The mechanism that causes this propagation is the interplay between the gradient and the curvature of the pressure profile. The onset of the oscillations prevents the system from undergoing an early transition to the enhanced confinement mode.

The extent and structure of the oscillations in the envelope of the fluctuation level depend on the details of the set of transport equations. The oscillations start when and where the system starts to undergo the phase transition, but the oscillations themselves prevent it by expelling the steep gradients to the region of high transport and convectively increasing the flux of heat and particles. If the power is further increased, the transition can take place. After the transition, the local time traces of the fluctuation level at the barrier position have a wide power spectrum. The dominant frequencies shift to higher values for increasing NBI powers (i.e., for increasing particle and heat flux through the transport barrier).

## ACKNOWLEDGMENTS

The authors wish to thank J-N. Leboeuf for numerous helpful comments.

This work has been sponsored by the Office of Fusion Energy, U.S. Department of Energy, under Contract No. DE-AC05-96OR22464.

<sup>1</sup>F. Wagner, G. Becker, K. Behringer *et al.*, Phys. Rev. Lett. **49**, 1408 (1982).

<sup>2</sup>K. Itoh and S. I. Itoh, Plasma Phys. Controlled Fusion **38**, 1 (1996).

<sup>3</sup>R. J. Groebner, K. H. Burrell, and R. P. Seradarian, Phys. Rev. Lett. **64**, 3015 (1990).

<sup>4</sup>K. H. Burrell, T. N. Carlstrom, E. J. Doyle *et al.*, Plasma Phys. Controlled Fusion **34**, 1859 (1992).

<sup>5</sup>P. H. Diamond, V. Shapiro, V. Shevchenko, Y.-B. Kim, M. N. Rosenbluth, B. A. Carreras, K. Sidikman, V. E. Lynch, L. Garcia, P. W. Terry, and R. Z. Sagdeev, Plasma Phys. Controlled Nucl. Fusion Res. **2**, 97 (1993).

<sup>6</sup>F. L. Hinton and G. M. Stabler, Phys. Fluids B **5**, 1281 (1993).

- <sup>7</sup>Y. Koide, M. Kikuchi, M. Mori *et al.*, Phys. Rev. Lett. **72**, 3662 (1994).
- <sup>8</sup>B. LeBlanc, S. Batha, R. Bell *et al.*, Phys. Plasmas **2**, 741 (1995).
- <sup>9</sup>M. Greenwald, D. Gwinn, S. Milora *et al.*, Phys. Rev. Lett. **53**, 352 (1984).
- <sup>10</sup>P. H. Diamond, V. B. Lebedev, D. E. Newman, B. A. Carreras, T. S. Hahm, W. M. Tang, G. Rewoldt, and K. Avinash, Phys. Rev. Lett. **78**, 1472 (1997).
- <sup>11</sup>T. S. Hahm, Phys. Plasmas **1**, 2940 (1994).
- <sup>12</sup>G. Staebler, Plasma Phys. Controlled Fusion **40**, 569 (1998).
- <sup>13</sup>E. J. Synakowski, Plasma Phys. Controlled Fusion **40**, 596 (1998).
- <sup>14</sup>A. Fukuyama, S. Takatsuka, S.-I. Itoh, M. Yagi, and K. Itoh, Plasma Phys. Controlled Fusion **40**, 653 (1998).
- <sup>15</sup>E. Mazzucato, S. H. Batha, M. Beer *et al.*, Phys. Rev. Lett. **77**, 3145 (1996).
- <sup>16</sup>C. L. Rettig, K. H. Burrell, R. J. La Haye, T. H. Osborne, W. A. Peebles, and R. J. Groebner, Plasma Phys. Controlled Fusion **36**, A207 (1994).
- <sup>17</sup>B. A. Carreras, V. E. Lynch, L. Garcia, and P. H. Diamond, Phys. Plasmas **2**, 2744 (1995).
- <sup>18</sup>V. B. Lebedev and P. H. Diamond, Phys. Plasmas **4**, 1087 (1997).
- <sup>19</sup>B. A. Carreras, D. Newman, P. H. Diamond, and Y.-M. Liang, Phys. Plasmas **1**, 4014 (1994).
- <sup>20</sup>D. E. Newman, B. A. Carreras, and P. H. Diamond, Phys. Plasmas **2**, 3044 (1995).
- <sup>21</sup>D. E. Newman, B. A. Carreras, D. Lopez-Bruna, P. H. Diamond, and V. B. Lebedev, Phys. Plasmas **5**, 938 (1998).
- <sup>22</sup>H. Biglari, P. H. Diamond, and P. W. Terry, Phys. Fluids B **2**, 1 (1990).
- <sup>23</sup>A. Yoshizawa, Phys. Fluids **27**, 1377 (1984).
- <sup>24</sup>P. H. Diamond, Y.-M. Liang, B. A. Carreras, and P. W. Terry, Phys. Rev. Lett. **72**, 2565 (1994).
- <sup>25</sup>T. S. Hahm and K. H. Burrell, Phys. Plasmas **2**, 1648 (1995).
- <sup>26</sup>G. Bateman, Phys. Fluids B **4**, 634 (1992).
- <sup>27</sup>H. Biglari, P. H. Diamond, and M. N. Rosenbluth, Phys. Fluids B **1**, 109 (1989).
- <sup>28</sup>R. J. Hawryluk, H. Adler, P. Alling *et al.*, Plasma Physics and Controlled Nuclear Fusion Research 1994 (International Atomic Energy Agency Vienna, 1995), Vol. 1, p. 11.
- <sup>29</sup>J. Y. Kim and M. Wakatani, Phys. Plasmas **2**, 1012 (1995).
- <sup>30</sup>G. Rewoldt, L. L. Lao, and W. M. Tang, Phys. Plasmas **4**, 3293 (1997).
- <sup>31</sup>G. Staebler, R. Waltz, and J. C. Wiley, Nucl. Fusion **37**, 287 (1997).
- <sup>32</sup>D. R. Ernst, M. G. Bell, R. E. Bell *et al.*, Phys. Plasmas **5**, 665 (1998).
- <sup>33</sup>Y. B. Kim, P. H. Diamond, and R. J. Groebner, Phys. Fluids B **3**, 2050 (1991).